Vorticity dynamics in a breaking internal gravity wave. Part 2. Vortex interactions and transition to turbulence

By DAVID C. FRITTS[1],
STEVE ARENDT[1] AND ØYVIND ANDREASSEN[2]

[1]Laboratory for Atmospheric and Space Physics, University of Colorado, Boulder, CO 80309-0392, USA

[2]Norwegian Defence Research Establishment, Kjeller, Norway

A companion paper (Part 1) employed a three-dimensional numerical simulation to examine the vorticity dynamics of the initial instabilities of a breaking internal gravity wave in a stratified, sheared, compressible fluid. The present paper describes the vorticity dynamics that drive this flow to smaller-scale, increasingly isotropic motions at later times. Following the initial formation of discrete and intertwined vortex loops, the most important interactions are the self-interactions of single vortex tubes and the mutual interactions of multiple vortex tubes in close proximity. The initial formation of vortex tubes from the roll-up of localized vortex sheets gives the vortex tubes axial variations with both axisymmetric and azimuthal-wavenumber-2 components. The axisymmetric variations excite axisymmetric twist waves or Kelvin vortex waves which propagate along the tubes, drive axial flows, deplete the tubes' cores, and fragment the tubes. The azimuthal-wavenumber-2 variations excite $m = 2$ twist waves on the vortex tubes, which undergo strong amplification and unravel single vortex tubes into pairs of intertwined helical tubes; the vortex tubes then burst or fragment. Reconnection often occurs among the remnants of such vortex fragmentation. A common mutual interaction is that of orthogonal vortex tubes, which causes mutual stretching and leads to long-lived structures. Such an interaction also sometimes creates an $m = 1$ twist wave having an approximately steady helical form as well as a preferred sense of helicity. Interactions among parallel vortex tubes are less common, but include vortex pairing. Finally, the intensification and roll-up of weaker vortex sheets into new tubes occurs throughout the evolution. All of these vortex interactions result in a rapid cascade of energy and enstrophy toward smaller scales of motion.

1. Introduction

Numerous observational and numerical studies in recent years have examined the transition to and the statistical structure within turbulent motions with particular emphasis on vortex structures (Rogers & Moin 1987; She, Jackson & Orszag 1990; Vincent & Meneguzzi 1991, 1994; Sandham & Kleiser 1992; Cadot, Douady & Coudet 1995; Metais *et al.* 1995). Indeed, the nature of the transition from laminar to turbulent flow remains one of the more compelling problems in fluid dynamics. Yet it has proven difficult to model the transition numerically with both a geophysical

source of turbulence and sufficient resolution to describe the important processes and interactions. The purpose of this paper is to provide such an analysis using a numerical simulation of a breaking internal gravity wave in a stratified and sheared fluid. Such waves are thought to be important sources of turbulence in the terrestrial and planetary atmospheres, in the oceans, and in stellar interiors.

Our initial studies of wave breaking focused on the character and energetics of wave instability and its effects on the wave and mean state using coarser model resolution (Andreassen *et al.* 1994; Fritts, Isler & Andreassen 1994; Isler, Fritts & Andreassen 1994; Fritts, Garten & Andreassen 1996). These studies, along with those of Winters & D'Asaro (1994), provided the first descriptions of the transition to three-dimensional structure in a breaking wave at smaller scales of motion in a stably stratified and sheared environment. The instabilities which result contribute importantly to wave dissipation and to eddy transports of momentum and heat within the fluid. However, these studies did not provide the resolution necessary to address the small-scale vorticity dynamics in detail.

More recently, a companion paper by Andreassen *et al.* (1998), hereafter denoted Part 1, has examined the vorticity dynamics accompanying the primary and secondary instabilities occurring within a breaking gravity wave at higher resolution. For relatively high-frequency ($\omega \leqslant N$) wave motions, the primary instability takes the form of counter-rotating streamwise† vortices driven by baroclinic sources within convectively unstable regions of the wave field. The streamwise vortices act on the adjacent environmental shears, causing the formation and intensification of spanwise vortex sheets. Continued stretching of these sheets causes them to become dynamically unstable, so that a series of small-scale, spanwise-localized, Kelvin–Helmholtz (KH) instabilities develops. The resulting vortex tubes evolve with their axes along the vorticity field of the vortex sheets (i.e. in the spanwise direction) and link continuously to the streamwise vortices accounting for sheet intensification. The result of these instability processes is a series of intertwined vortex loops, closely resembling the 'horseshoe' or 'hairpin' vortices observed in boundary layer flows and sheared homogeneous or stratified turbulence (Robinson 1991; Sandham & Kleiser 1992; Gerz, Howell & Mahrt 1994; Metais *et al.* 1995). Thus, the interactions of the loops we observe are likely to be representative of such turbulent transitions in many flows.

During the transition to smaller scales, the vortex loops exhibit a spectrum of interactions and dynamics, many of which have been observed in laboratory studies or previous numerical simulations, but which are, for the most part, not well understood at present. For example, oscillations of vortex tubes have been studied in the laboratory (Hopfinger, Browand & Gagne 1982; Maxworthy, Hopfinger & Redekopp 1985) and in numerical simulations (Melander & Hussain 1994, 1995; Schoppa, Hussain & Metcalfe 1995). These oscillations are copiously present in our simulation and appear to be manifestations of Kelvin vortex waves, or twist waves, first discovered by Kelvin (1880). Twist waves are excited by both the initial state of a vortex tube (Arendt, Fritts & Andreasson 1997) and by mutual interactions with neighbouring tubes. In our simulation, the waves lead to the unravelling and fragmentation of the vortex tubes; laboratory studies have demonstrated similar events (Cadot *et al.* 1995). Reconnection events, which have been studied in many contexts (Pumir & Siggia 1990; Boratav, Pelz & Zabusky 1992; Shelley, Meiron & Orszag 1993), are likewise present.

† As in Part 1, the two horizontal orthogonal directions x and y will be referred to as streamwise and spanwise respectively. The initial wave propagation is streamwise (with a small vertical component), as is the background shear flow. The vorticity of the background shear flow is then spanwise.

Our purpose in this paper is to understand the vorticity dynamics and evolution subsequent to the primary convective and secondary dynamical instabilities examined in Part 1. Specifically, we will evaluate the perturbations to and the interactions among the vortex loops resulting from the initial flow instabilities. These interactions drive the evolution toward smaller scales and more chaotic and isotropic structure. An overview of the enstrophy and vortex evolutions during this latter phase of wave breaking is presented in §2. Section 3 examines in greater detail several processes that appear to play major roles in the cascade toward smaller scales. These include vortex sheet intensification and roll-up, orthogonal vortex stretching, and mode-zero and -two twist waves on the vortex tubes. Section 4 describes additional interactions which appear to be significant in, but less central to, the vortex morphology, including mode-one twist waves, pairing events among aligned and closely spaced tubes, and viscous reconnection of vortex tubes or fragments in close proximity. A description of the enstrophy spectra and of viscous influences at small scales is presented in §5. Our conclusions and a discussion of the relevance of these results to general sheared turbulence studies are presented in §6.

2. Enstrophy and vortex evolution

In this section, we provide an overview of the enstrophy and vortex morphology in the wave breaking simulation extending from $t = 70$ to 80, approximately 0.7 buoyancy periods† beyond that described in Part 1. Figure 2(*d*) in Part 1 at $t = 70$ reveals a field of intertwined and increasingly interacting vortex loops (using λ_2 of Jeong & Hussain 1995, as discussed in Part 1) arising from the primary convective and secondary dynamical instabilities. The further evolution of this field is displayed in figure 1(*a–d*) at $t = 72.5$, 75, 77.5, and 80. The increase in flow complexity is dramatic. The vortex loops present at $t = 70.0$ are fragmented into pieces, and new smaller vortex tubes continue to be formed (small blue and grey wisps in figure 1). At later times, apart from a large-scale correlation with the phase of the original gravity wave, the small-scale flow is almost isotropic, and has little evidence of its initial state. The vortices lose their initial streamwise and spanwise orientation and structures appear at significantly higher wavenumbers (by a factor of 2 to 3), as will be discussed in §5. Also, the maximum vorticity and enstrophy at small scales of motion increase throughout the simulation (see figures 7 and 8 of Part 1).

In order to examine the relationship between enstrophy and the vortices defined by λ_2, we now focus on a subdomain at the upper left of the images in figure 1. This subdomain is shown in figure 2 for $t = 70$ to 75. Here, the enstrophy is pink (shown for values of 25.0 and higher; a typical background enstrophy is 5.0–10.0), and λ_2 is yellow for large negative values and blue for small negative values. In part (*a*), we see four prominent spanwise vortices at various stages of development and interaction. All four have arisen due to KH instability of initial spanwise vortex sheets, as addressed in Part 1. The two vortices on the left have formed on the same sheet, while the two vortices on the right have formed on distinct vortex sheets and are in a more advanced stage of interaction with their neighbours. As time proceeds, the vortex tubes unravel and break into fragments. Consider the left-most vortex for example. By $t = 73.0$, this vortex is beginning to unravel, and by $t = 75.0$, it has become an intertwined pair of helices. This effect is common in our simulations (see e.g. the centremost tube in figure 2), and will be discussed in the context of twist waves in §3.4.

† The times are normalized to the sound crossing time of a density scale height. With this normalization, the buoyancy period is 14.
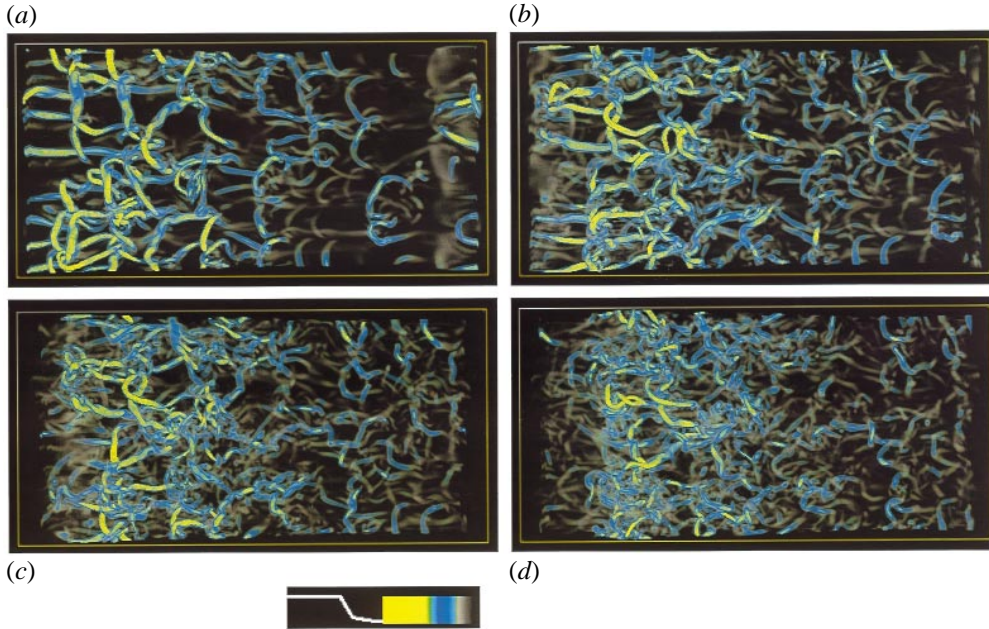
(*a*)   (*b*)

(*c*)   (*d*)

FIGURE 1. Volume renderings of λ_2 from below with positive x to the right at (*a*) $t = 72.5$, (*b*) 75, (*c*) 77.5, and (*d*) 80. Colour and opacity scales are shown at the lower left. The opacity scale extends from transparent to opaque; both scales show negative λ_2 with zero at the right.

The enstrophy is seen to be largely associated with the evolving vortex tubes throughout this evolution, although there is still some enstrophy that is distinct from the vortex tubes, and is sheetlike rather than tubelike (see the hazy pink areas figure 2*a*). This contrasts with earlier times in the wave breaking where the enstrophy was mostly confined to sheets (see figures 2 and 3 of Part 1). As the evolution progresses, some of the enstrophy sheets are stretched by neighbouring vortices, intensify locally, and roll-up into vortex tubes. This process is seen at several sites in figure 2. One such event occurs from $t = 70$ and 71 (figure 2*a,b*) just to the left of the lower end of the spanwise tube near the centre of these images. This sheet has no λ_2 signature at $t = 70$, but contains a weak streamwise vortex (shown in λ_2) at $t = 71$ which intensifies in subsequent images and attaches to the adjacent spanwise tube. Another example occurs from $t = 71$ and 72, where a strong spanwise vortex tube arises on the enstrophy sheet at the lower left of the image at $t = 71$. Additional vortices arise in the same manner in other locations, in each case on weaker vortex sheets and at smaller scales, until virtually all of the enstrophy with a magnitude sufficient to be displayed is associated with vortex tubes. Thus vortex sheet intensification and roll-up remains an important process throughout this flow evolution, as it probably is in other turbulent flows as well (Betchov 1957; Lundgren 1982).

3. Primary vortex dynamics

In evaluating the vortex dynamics accompanying the evolution toward smaller scales and increasing isotropy, we have identified several processes that appear to be important. The discussion in this section addresses the vortex dynamics that we judge
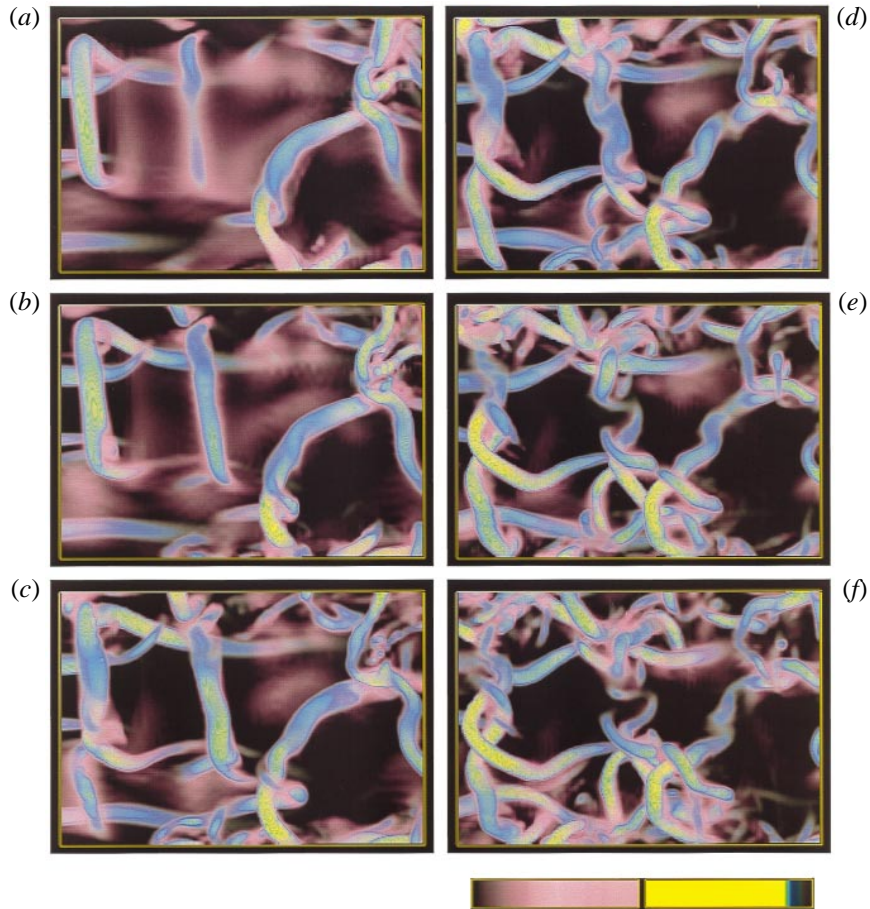
FIGURE 2. Two-field renderings of enstrophy and λ_2 viewed from below with positive x to the right from $t = 70$ to 75 (a–f) in a subdomain at small x and small y (the upper left corner of the views from below in figure 1). Colour scales are shown at the lower right.

to be key to the transition to and the cascade within a turbulent flow. Other vortex interactions that participate in the transition, but are judged to be less important, are described in the following section.

3.1. *Orthogonal vortex stretching*

The key element in vortex intensification on short time scales is vortex stretching, either of the ambient shear field by localized vortices (or vice versa) or of localized vortices by other localized and closely spaced vortex structures. For this process to be effective, the local component of vorticity, ω_i, and the diagonal component of the strain tensor, S_{ii}, must contribute a source, $\omega_i S_{ii}$, which exceeds other baroclinic, compressional, and viscous contributions. This stretching source is particularly strong when the vorticity lines of two neighbouring vortex structures are nearly orthogonal. Physically, the stretching is due to a flow divergence along the vorticity. Because of the geometry of the flow, vorticity is stretched on the upstream side (relative to the point of closest approach) of an orthogonal vortex, and scrunched on the downstream side. (We will use the term scrunching for weakening or negative-stretching of vorticity due to local flow convergence.) This mutual stretching (and scrunching) is illustrated schematically,
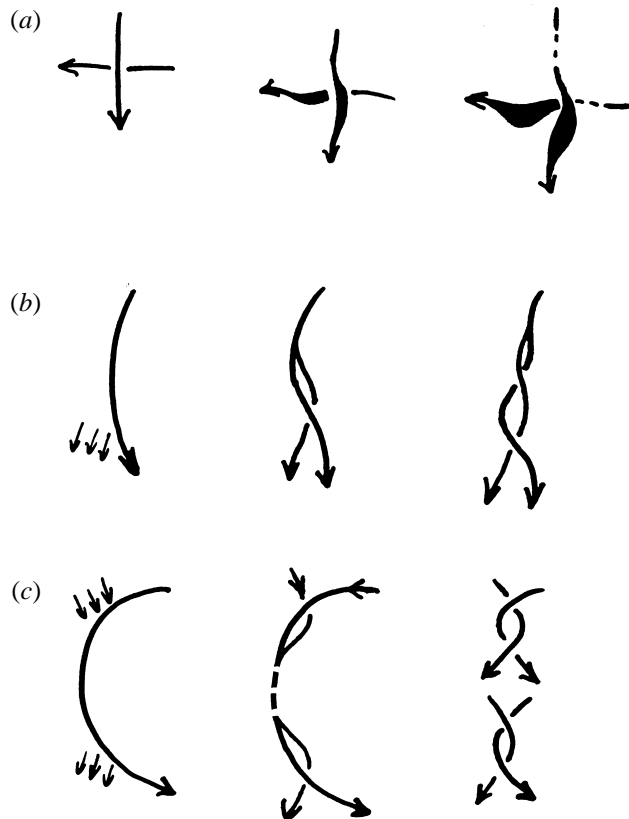
FIGURE 3. Schematics of three of the primary vortex interactions which account for the dominant vortex structures and drive the cascade of enstrophy toward smaller scales. Series (*a*) illustrates the differential stretching and scrunching of orthogonal, mutually interacting vortices leading to intensification and long-lived *x*-patterns structures. Series (*b*) illustrates the intensification of a weak vortex sheet, its attachment to a stronger vortex tube, and the subsequent twist wave amplification, propagation, and fraying under unstable conditions (see text for details). Series (*c*) illustrates the impact of mode-two twist waves initiated at different sites on a vortex tube that propagate toward each other and result in the unraveling and breakup of the vortex tube.

with vortex thickness indicating strengthening and dashed lines denoting weakening, in figure 3(*a*).

Noting that the vorticity lines of the vortex sheets are predominantly spanwise (vertical in figure 2) and that the vorticity lines of a vortex tube are roughly along the tube, we note that there are indeed numerous sites where vortex structures in figure 2 have approximately orthogonal alignments and undergo local intensification. When the stretching involves a vortex sheet, roll-up and tube formation can result, as discussed in §2 and §3.2. An important consequence of this mutual stretching is the preferential amplification of the orthogonal vortex structures, causing these structures to become most prevalent as the field evolves. Indeed, these 'x-patterns' appear as frequent and persistent features in the vortex evolution and can be seen surviving to late times relative to other features of the flow in figure 1. Additional examples can be seen in figure 6 and will be discussed further below. Such 'x-patterns' were observed by Boratav *et al.* (1992) and Pumir & Siggia (1990) to lead ultimately to anti-parallel vortex alignments at late times in an unstratified flow. However, late-time

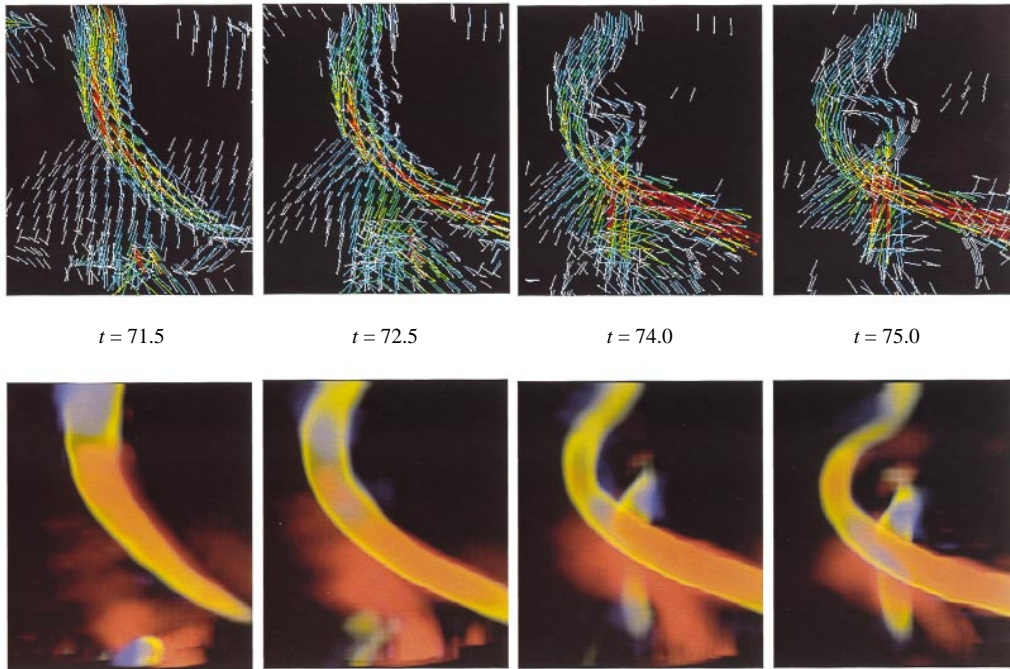| $t = 71.5$ | $t = 72.5$ | $t = 74.0$ | $t = 75.0$ |

FIGURE 4. Volumetric views of the vorticity field viewed from below with positive x to the right in a small subdomain in the lower central region of the images shown in figure 1. Upper panels show the vorticity vectors (with white/blue weak and red/yellow strong). Lower panels show vortex tubes rendered with λ_2 in yellow and having transparent cores and the sources and sinks of enstrophy due to stretching, with positive (negative) red (blue). Times are $t = 71.5$, 72.5, 74 and 75.

anti-parallel alignments are not observed in our flow, perhaps as a result of the more viscous nature of the vortex dynamics in our simulation.

3.2. *Vortex sheet and tube formation*

Formation and intensification of vortex sheets and their subsequent roll-up into vortex tubes were identified as initial steps in the transition to and within turbulent flow by Betchov (1957) and Lundgren (1982). Our results in Part 1 and the previous discussion of figure 2 show that these processes also occur in a stratified fluid and play a continuing role throughout the flow evolution. Sheet roll-up occurs on sheets which have been intensified by vortex stretching from the flow of a neighbouring orthogonal vortex, as discussed above. The roll-up proceeds by analogy with the two-dimensional KH instability of an infinite vortex sheet studied by many authors or the three-dimensional KH sheet instability described in Part 1.

A specific example of the intensification and roll-up of a vortex sheet due to its proximity to an adjacent vortex tube is shown in figure 4 with vorticity vectors in the upper row, and with volumetric views of vortex tubes and sources/sinks of enstrophy due to stretching in the lower row. Vorticity vectors having small magnitudes (3.0–4.0) are coloured white/blue, while those having large magnitudes (6.0–8.0) are coloured red/yellow. Vortex tubes, which are defined by λ_2 are coloured yellow, and are given transparent cores so that the sources within are visible. The positive/negative sources of enstrophy due to stretching are coloured red/blue (at values in excess of ± 12.0). The initial structure displayed is located in the upper left central portion of figure 1(*a*).

At $t = 71.5$ in figure 4, a weak vortex sheet (displayed in white vectors) overlies

a prominent vortex tube (displayed in yellow λ_2). The vorticity vectors of the sheet and the tube are approximately orthogonal. As the evolution progresses, this vortex sheet intensifies due to stretching by the underlying vortex tube. This can be seen clearly as a positive (red) source of enstrophy at the location of the vortex sheet at $t = 72.5$, and an increase in the magnitude of the vorticity vectors comprising the sheet (note the appearance of blue and green vectors). Continued stretching by the vortex tube intensifies the vortex sheet locally, until it rolls up via the KH instability. Noting that the dynamical timescale of a shear layer is $t \sim (\mathrm{d}U/\mathrm{d}z)^{-1} = \omega^{-1}$ which is roughly $t \simeq 0.2$ for this sheet, we see that the roll-up of the sheet takes 5–10 shear timescales. Having rolled up, it achieves the local rotational character necessary for it to appear as a vortex tube in λ_2 (see the short yellow tube at $t = 74$ and 75). The roll-up of this vortex sheet has led to the creation of a new vortex tube with a strength comparable to the tube responsible for its intensification. The vector fields at $t = 74$ and 75 also show a tendency for the emerging vortex tube to attach to the sheath of the initial tube in a helical fashion. This process will be examined in greater detail in §3.4.

3.3. *Mode-zero twist waves*

We noted earlier that the vortex loops arising from the secondary KH instability tend to fragment into pieces. One of the causes of this fragmentation is the presence of mode-zero twist waves of large amplitude. Figure 5 shows an example of such a wave on a single span-wise vortex tube. Figure 5(*a–e*) show λ_2 at successive times with opaque green/blue being the largest magnitude and wispy grey being the smallest magnitude. Figure 5(*f–h*) show the vorticity vectors (ranging in magnitude from 3.0 to 8.0 – all coloured dark blue), isosurfaces of enstrophy sources/sinks due to stretching (± 15.0 coloured red/light-blue respectively), and vorticity lines (yellow) at several times corresponding to the first, second, and fourth λ_2 images (figure 5*a*, *b*, *d*). The vorticity lines shown are not the same lines in each panel; rather, in each individual panel, lines are chosen to give a sense of the vorticity topology as a whole.

Concentrating first on the λ_2 images, we see that at $t = 70.5$ (figure 5*a*), the tube is strongest in λ_2 near the ends. As time progresses, λ_2 becomes stronger everywhere along the tube except at the upper end, where it weakens (see $t = 71.5$ and 72.0). At later times, the tube begins to bend in the middle ($t = 72.5$), and then becomes depleted in the middle and unravels at the ends.

To understand this evolution, consider the panels showing the vorticity lines and enstrophy sources/sinks. In the first and second of these (figure 5*f*, *g*), one sees that the vorticity lines are slightly twisted near the top of the vortex tube and, to a lesser extent, near the bottom of the tube. This is because the ends of the parent vortex sheet roll up to become the ends of the vortex tube sooner than the middle of the sheet rolls up to become the middle of the tube. The twisted vorticity induces an axial (i.e. along the tube) flow which, in turn, strengthens/weakens the vorticity where the flow diverges/converges along the axis. The vorticity in the lines is pointed downward in figure 5, so at $t = 71.5$ the axial flow is from the middle of the tube and toward the upper end (one can use the Biot–Savart law or the right-hand rule to see this). This produces the red enstrophy source in the middle of the tube at $t = 71.5$ and the blue enstrophy sink above it. The enstrophy source strengthens the tube in the middle, so that at a later time, the middle of the tube rotates faster than the ends and the sense of twist of the vorticity lines reverses; note that the sense of the twist of the vorticity lines at $t = 72.5$ in figure 5(*h*) is opposite that at $t = 71.5$. When the twist reverses, the axial flow, as well as the flow's enstrophy sources/sinks, also reverses; in figure 5 the

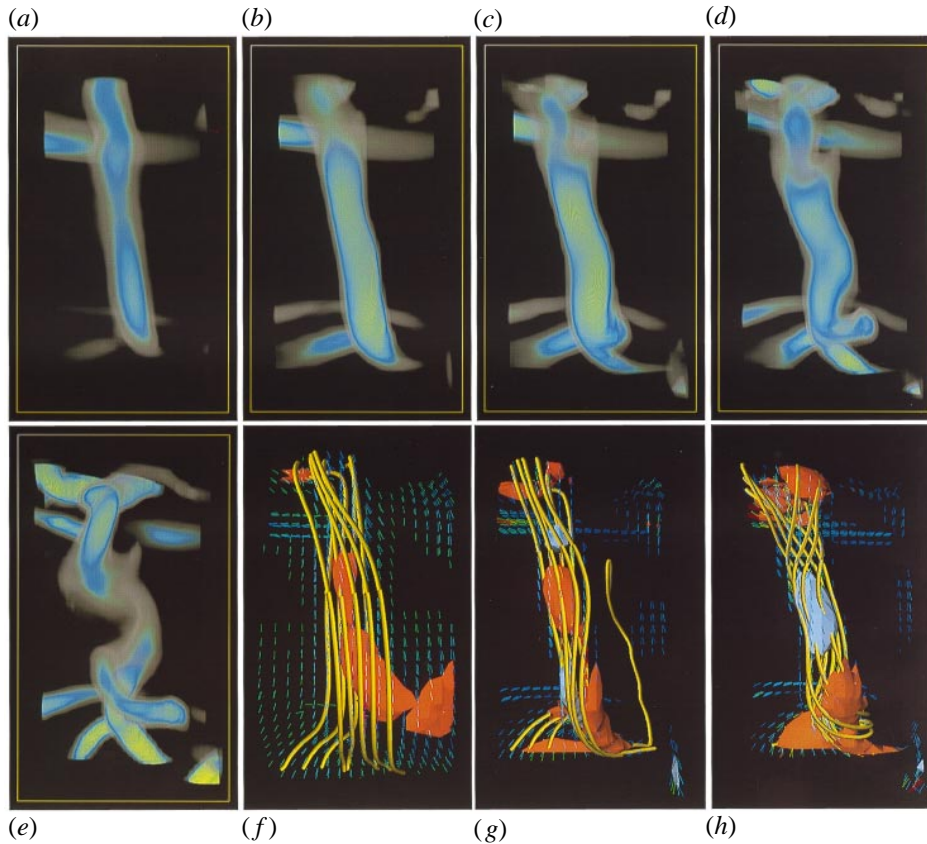(*a*) (*b*) (*c*) (*d*)

(*e*) (*f*) (*g*) (*h*)

FIGURE 5. Detail of the λ_2 evolution exhibiting formation and breakup of the spanwise vortex tube at the centre of the subdomain shown in figure 2 at (*a*) $t = 70.5$, (*b*) 71.5, (*c*) 72, (*d*) 72.5, and (*e*) 73.5. Additional images illustrate the twisted vorticity fieldlines and the enstrophy sources and sinks (red positive and blue negative) due to twist wave propagation which account for vortex breakup at (*f*) $t = 70.5$, (*g*) 71.5, and (*h*) 72.5. Colour and opacity scales for λ_2 are as in figure 1.

enstrophy source in the middle of the tube at $t = 71.5$ is replaced by an enstropy sink at $t = 72.5$. Although it is not shown in figure 5, the magnitude of the inward axial flow responsible for this sink is about 0.05. This enstrophy sink weakens the middle of the tube, so that at later times the tube fragments, as seen in λ_2 at $t = 73.5$. The tube is simultaneously unravelling from the ends in a process which will be discussed in §3.4.

Similar events on other spanwise vortex tubes are observed elsewhere within the wave breaking simulation, suggesting that this is an important process in the flow evolution. In most cases, however, the initial vortices are stronger near the middle rather than near the ends as above because the middle of the parent vortex sheets rolls up faster than the ends. The final result is nonetheless the same, with the twist inducing an inward axial flow, and the flow, in turn, leading to enstrophy depletion in the middle of the vortex tube, and, ultimately, fragmentation.

The sequence of events described above is also responsible for the propagation of $m = 0$ twist waves along a vortex tube, as first described by Kelvin (1880). Similar dynamics of a vortex tube were recently described in some detail by Melander & Hussain (1995) and Schoppa *et al.* (1995) in association with vortex core dynamics. In

(*a*) (*b*) (*c*) (*d*) (*e*)
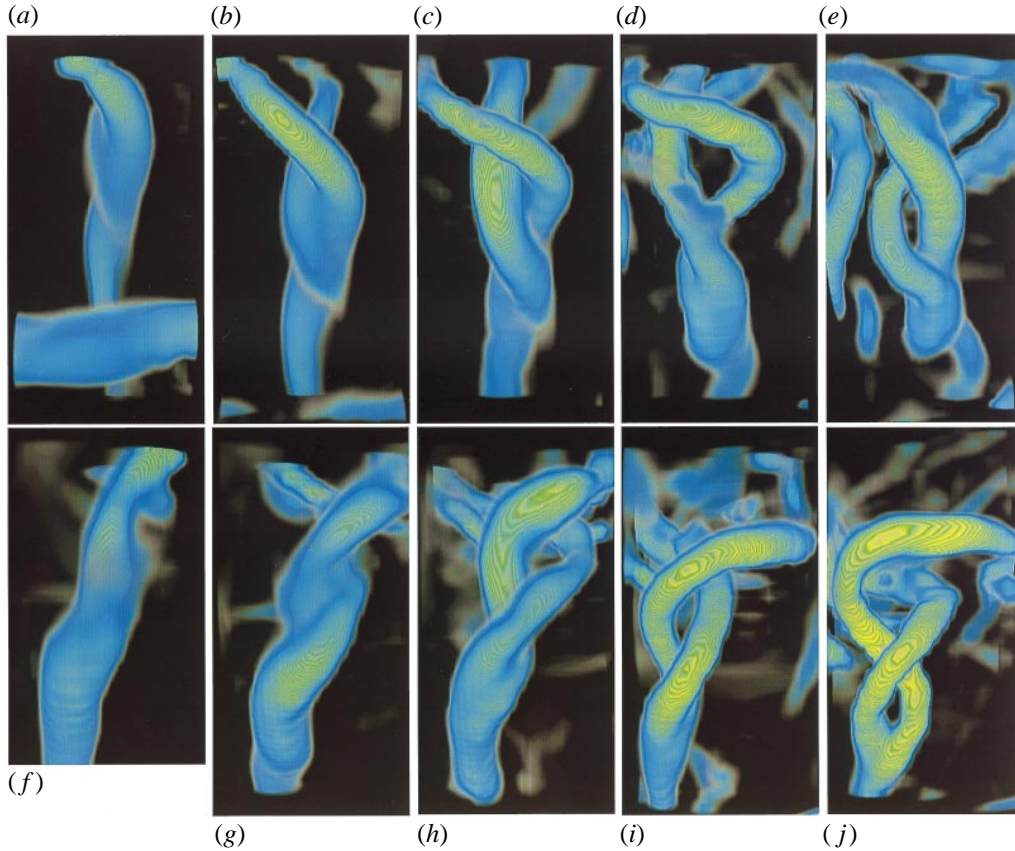

(*f*)

(*g*) (*h*) (*i*) (*j*)

FIGURE 6. As in the λ_2 images in figure 5 showing the unravelling of two streamwise vortex tubes due to propagation of mode two twist waves on vortex tubes having negative (upper series, *a–e*) and positive (lower series, *f–j*) streamwise vorticity: (*a–e*) times $t = 72$ to 76, (*f–j*) times $t = 75$ to 79. In each series, the images display the amplification and propagation of an $m = 2$ wave packet, and the consequent fraying of the vortex tube into a double helix.

general, twist waves are dispersive travelling waves on vortex tubes. The axisymmetric ($m = 0$, where m is the azimuthal wavenumber of the wave) modes propagate by twisting the vortex lines of the tube, thereby creating an axial flow. The axial flow changes the enstrophy of the tube by stretching/scrunching. This, in turn, changes the rotation rate of the tube which then changes the twist. From this point of view, the event shown in figure 5 is a standing axisymmetric twist wave on a vortex tube excited by the initial state of the tube (Arendt *et al.* 1997). The wave is of such large amplitude that it irreversibly depletes the middle of the vortex tube during its minimum. Azimuthal modes of higher m also exist. Of particular importance for our results are $m = 2$ modes which are responsible for the unravelling of vortex tubes into pairs of intertwined helices; this will be discussed in the next subsection.

3.4. *Mode-two twist waves*

A type of twist wave which plays a major role in the fragmentation of vortex loops is a mode two ($m = 2$) wave. These waves are generally excited where a vortex tube is perturbed near its end by another vortex structure (either a tube or sheet). The clearest and most long-lived examples of mode-two twist waves in our numerical

solution arise due to upstream perturbations of the more axially uniform streamwise vortex tubes. Two of these waves are in the upper left portions of the images shown in figure 1. They are shown magnified in figure 6, with the evolution of λ_2 for the two different waves shown in the upper and lower rows of panels. The view is from below with positive x (the streamwise direction) downward. In each case, a streamwise-propagating $m = 2$ twist wave with a small amplitude is excited on the vortex tube; the propagation of the wave is not seen since the domain displayed is adjusted to track it. The waves grow until they are sufficiently large to unravel the vortex tube into a pair of intertwined helices; a schematic of this is shown in figure 3(*b*). The vorticity of the tubes is roughly 6.0, so that the circulation times of the two tubes are $\tau = 4\pi/\omega \simeq 2.0$. From figure 6 then, the growth of the wave takes about one circulation time. Figures 3 and 4 of Arendt *et al.* (1997) show analytic examples of propagating $m = 2$ twist wave packets excited by initial perturbations of the vortex tubes. That calculation is linear, and so it cannot lead to an unravelling of the vortex tube, but the same intertwined helix structure is observed.

It is useful to understand how an $m = 2$ wave propagates. Essentially, such a wave is propelled by self-advection, i.e. the vortex tube induces a velocity field, and is then advected by it. This is a common effect in vortex dynamics; a simple example is that of a vortex ring which is propelled in a direction perpendicular to its plane by its own velocity field. In the case of an $m = 2$ wave, each helix of the pair induces a velocity field with both an azimuthal rotating component and an axial component. The axial component propels the wave by advecting the helices. For example, the tube shown in figure 6(*a–e*) has vorticity vectors pointing upward (not shown). Given the sense of the helices of the wave, it is easy to show (using the Biot–Savart law or simply the right-hand rule) that the axial velocity is downward, and so the wave propagates downward. At the head of the wave packet, where the tube is unsplit, the axial flow of the approaching double helices precedes the helices themselves. The axial flow decays with distance from the helices, and so it is convergent along the axis in front of the wave. If the flow converges axially, it must diverge radially; this radial divergence splits the vortex tube into the two component helices.

An important consequence of the self-advected propagation of an $m = 2$ wave is that the direction of propagation is determined by the direction of the vorticity in the tube and the sense of the helices of the wave packet. These two components determine the direction of the axial flow, and hence the direction of propagation. In the two examples in figure 6, the direction of the vorticity (not shown) is opposite for each, being upward in the top example and downward in the bottom example. Since the sense of the helices is also opposite for each, as is shown in figure 6, both waves propagate downward. This effect is also apparent in Plates 3 and 4 of Arendt *et al.* (1997). There, an initial small split in the middle of a vortex tube produces two wave packets propagating outward from the split in opposite directions. The two wave packets share the same direction of vorticity since they occupy the same vortex tube, but they have opposite senses of helicity and so they propagate in opposite directions.

Another example of $m = 2$ twist waves is shown in figure 7. Here, the evolution of λ_2 for a spanwise vortex loop is shown in (*a–e*). As in figure 5, the last three panels (*f–h*) show vorticity vectors (having magnitudes greater than 4.0), vortex lines, and enstrophy sources/sinks (isosurfaces of ± 30.0) for the first, third, and fourth λ_2 panels. Consider first the λ_2 evolution. After the dominant spanwise vortex loop forms ($t = 69$, figure 7*b*), structures which underlie it and which are initially weak, intensify (especially at the lower end of the tube) and appear to attach to the spanwise vortex loop at $t = 70$–71 (although we will show that the lines comprising the weak
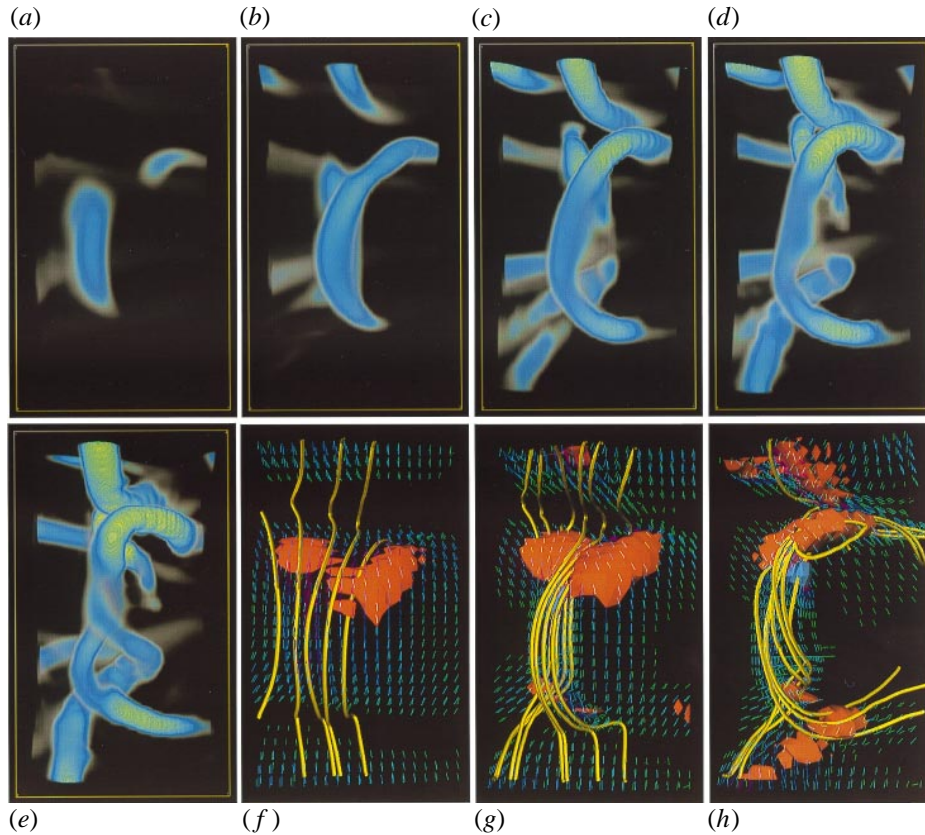
FIGURE 7. As in figure 5 displaying vortex formation, attachment, mode-two twist wave excitation and propagation, and vortex unravelling for a vortex seen at the lower left of figure 3(*d*) of Part 1 and figure 1(*a*). Successive λ_2 images are at times (*a*) $t = 68$, (*b*) 69, (*c*) 70, (*d*) 70.5, and (*e*) 71. The remaining images are as in figure 5 at (*f*) $t = 68$, (*g*) 69, and (*h*) 70.

vortex are already attached to the main vortex) and cause the loop to unravel. This process is just the inward propagation of two $m = 2$ twist waves along the loop. A schematic of the vortex loop unravelling at both ends is shown in figure 3(*c*) to guide the interpretation of figure 7. The initial perturbations to the ends of the loop in figure 7 generate $m = 2$ waves which propagate inward toward the middle of the loop. In doing so, they unravel the loop into intertwined helices, as in the case shown in figure 7. A similar event occurs in figure 5 and accounts for the unravelling seen there.

To support this interpretation and to study the initial excitation of the $m = 2$ waves, consider the vortex line evolution in figure 7(*f–h*). As before, the lines of vorticity are not the same in each panel, but rather are chosen to give a sense of the vorticity field topology at each time. Initially, vortex lines are distributed uniformly over the vortex sheet ($t = 68$). Following the secondary KH instability discussed in Part 1, the sheet rolls up into a tube ($t = 70$). The vortex lines are gathered into the tube, but at the ends of the tube the vortex lines spread out again, so that the tube resembles a frayed string. The vorticity at the frayed ends is also being intensified (note the red enstrophy source, particularly that at the lower end of the vortex loop) because some of the lines are orthogonal to each other and so stretch each other. At a later time

($t = 70.5$), the lines at the ends of the tube are gathered into two distinct groups, one comprising the main vortex loop, and the other forming the second vortex discussed above. The mutual advection of the two groups of lines drives the groups apart, splitting the end of the tube and producing the $m = 2$ wave which travels inward. In this case the axial flow speed corresponding to the wave is roughly 0.08. Note the correspondence at $t = 70.5$ between the unravelling in the λ_2 image and that in the vortex line image; the structure which appears to attach to the vortex loop in the λ_2 image is actually already connected to it by vorticity lines. To summarize then, the vortex loop unravels because its initial formation leaves it with 'frayed' ends; these ends intensify and excite $m = 2$ twist waves which propagate inward along the tube, unravelling it as they go. These events are very common throughout our simulation. Similar unravelling events have been observed in the laboratory (Cadot *et al.* 1995) and may also be due to large-amplitude twist waves.

4. Secondary vortex dynamics

In this section we discuss several processes which play clear roles in the evolution of the vortex field due to wave breaking, but which appear to be of minor importance to the cascade of energy and enstrophy to smaller scales of motion. These include vortex reconnection, mode-one twist waves, and vortex pairing. Of the three, reconnection is easily the most pervasive, but perhaps the most difficult to quantify. Mode-one twist waves, in contrast, are easily seen in the numerical solution, arise from perturbations to vortex tubes, and can be described simply in terms of linear theory. Finally, vortex pairing arises when two spanwise loops are close to each other and proceeds in a manner analogous to such pairing events in two-dimensional flows.

4.1. *Vortex reconnection*

Reconnection events fall into two broad classes. The first are those described by Kida & Takaoka (1994) in which vortex tubes undergo attachment without requiring viscous reconnection of vortex fieldlines. An example of this sort of event is shown in the λ_2 images in figure 6 where the weaker tube at the bottom of the images attaches to the main spanwise vortex tube. However, as shown in figure 6 and as discussed previously, the two tubes are already connected by vorticity lines, so there is no reconnection of fieldlines. Examples of this sort are common in our simulation and are easy to spot through a close examination of figure 1.

The second class of reconnection events, those in which vortex fieldlines reconnect, has been a topic of detailed study (Pumir & Siggia 1990; Boratav *et al.* 1992; Shelley *et al.* 1993). An example of such an event occurring in our simulation is displayed in figure 8 with λ_2 shown in the upper panels and vorticity vectors and fieldlines in the lower panels. The vortex structure on which we focus is the dominant loop seen at the upper left at $t = 65$ and 67.5 in figure 2 of Part 1. This example involves the breaking of one initially continuous vortex loop and the reconnection of the upper segment of this vortex loop with a vortex tube arising on an adjacent vortex sheet. The initial vortex loop is shown in figure 8(a, e) at $t = 68$. An adjacent vortex is seen to emerge and strengthen behind (below in figure 8) the initial vortex loop from $t = 70$ to 71. As this lower vortex underlies the vortex loop, the stretching and scrunching due to their approximately orthogonal orientation enhances the leftmost part of the loop and weakens the rightmost part just where the vortex loop itself is undergoing a breakup (see figure 8c). At the last time ($t = 72$), the leftmost part of the vortex loop has connected with the lower vortex.

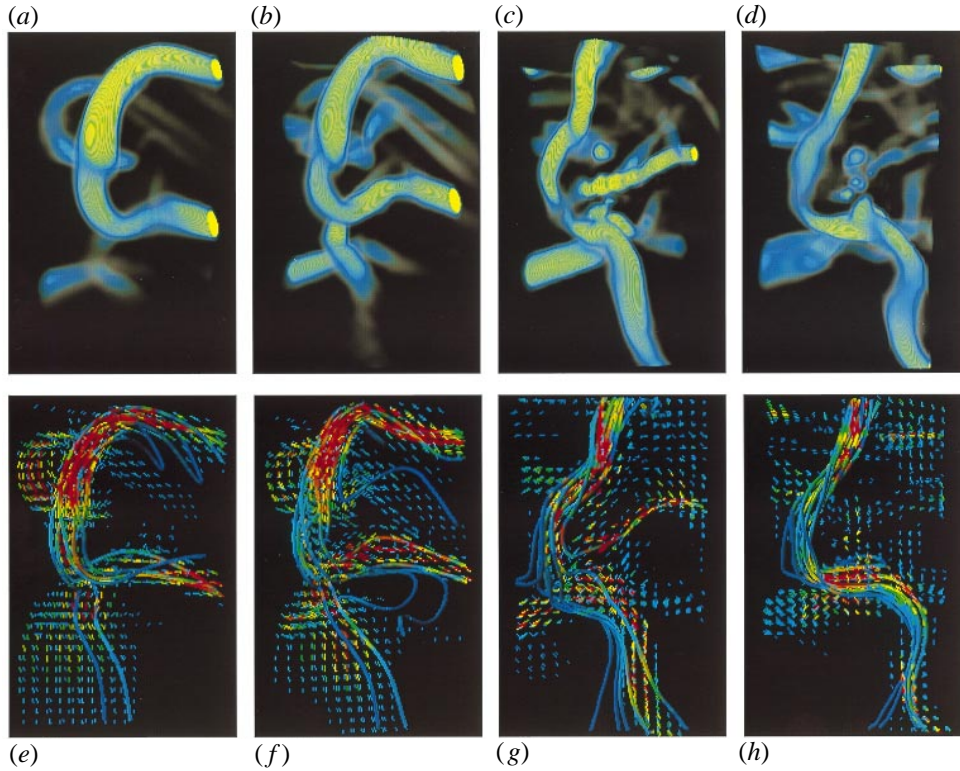(*a*) (*b*) (*c*) (*d*)

(*e*) (*f*) (*g*) (*h*)

FIGURE 8. As in figure 5 displaying vortex separation and reconnection for the vortex structure seen at the far right in the early images in figure 2 at times $t = 68$, 70, 71, and 72. The upper panels (*a–d*) show λ_2 while the lower panels (*e–h*) show vorticity vectors and fieldlines at the same times.

This sequence of events is supported by the parallel time series of the vorticity fieldlines in figure 8(*e–h*). The vorticity lines are coloured by the local strength of the vorticity with red corresponding to $\omega = 8.0$ and blue corresponding to $\omega = 4.0$. Initially at $t = 68$, most of the fieldlines passing through the vortex loop are confined to the vortex loop, and do not enter the lower vortex. This remains the case at $t = 70$ as the lower vortex strengthens. But as the vortex loop breaks up at $t = 71$, an increasing number of the fieldlines through the initial vortex loop attach or reconnect to the stronger lower vortex. At the last time shown, $t = 72$, all of the vorticity fieldlines have reconnected between the vortex loop and the lower vortex tube, while the severed portion of the initial loop has largely decayed away.

4.2. *Mode-one twist waves*

A final type of twist wave present in our numerical solution is the mode-one ($m = 1$) twist wave. This wave perturbs a vortex tube into a single helix and propagates through self-advection, as in the $m = 2$ case. An example of an $m = 1$ twist wave is present in figure 2, on the vortex tube that slants at about $45°$ in the images. At the earliest time shown, $t = 70$, the tube is unperturbed, but is frayed at its lower end. At a later time, $t = 74$, the tube is bent into a wiggling pattern; a close examination reveals that this is a helix. The wave is apparently excited by the close orthogonal neighbouring vortex underlying it at its lower end. The flow of this orthogonal neighbour bends the tube into a single wiggle (see $t = 72$), and the self-dynamics of

the tube transforms the single wiggle into a full helix. As the vorticity in that tube is about 6.0, the circulation time is about 1.0, so we see that the transformation to a full helix takes a few circulation times. Curiously, the wave does not seem to propagate. Rather, it appears to be a standing wave made stationary by the fact that the forcing causing it (i.e. the neighbouring orthogonal vortex) is stationary. Alternatively, the mode-one twist wave may be a true stationary wave, as such waves do occur (Saffman 1992); however a true stationary $m = 1$ wave has considerable radial structure within the tube, and we find no evidence of this.

Mode-one twist waves are observed to be excited in our numerical solution at a number of sites and times. Three clear examples are seen in figure 1(a) near the top centre, at the lower edge of the domain about 1/3 of the distance from left to right, and just above the latter structure and above the midpoint of the domain. Additional examples are seen further downstream (to the right, and toward positive x) and arising at later times in the evolution.

4.3. *Vortex pairing*

Vortex pairing, the mutual interaction of two parallel vortex tubes, is generally understood on the basis of two-dimensional laboratory and numerical studies. This process is often observed at a sheared interface in fluids that are homogeneous or have a density gradient confined to the shear layer (Scotti & Corcos 1972; Patnaik, Sherman & Corcos 1976; Koop & Browand 1979; Fritts 1984; Thorpe 1985; Metcalfe *et al.* 1987), and can be viewed as a degenerate resonant triad interaction between the primary KH billow and its subharmonic (Davis & Peltier 1979). Pairing is less pronounced in a fluid that is stratified away from the shear layer, however, for two reasons. First, the mean state Richardson number required for linear subharmonic instability, and hence for efficient subharmonic excitation, is much less than for the primary instability (Drazin 1958). Second, subharmonic excitation at larger Richardson numbers is suppressed because the subharmonic has propagating rather than evanescent character away from the shear layer and therefore radiates away as it is excited (Fritts 1984). As a result, such pairing events are not observed in the stratified atmosphere and oceans.

We observe several cases of vortex pairing in our results. Generally they resemble their two-dimensional analogues, with the vortices approaching closely, mutually advecting, and wrapping around each other. Pairing is different in three-dimensions in two respects. First, the vortex sheets are localized in the spanwise direction, and the resulting tubes are as well. At later times, the tubes are curved into loops with the streamwise extensions of the loop legs coming close together. So, the pairing proceeds between adjacent loops, with one loop (typically the upstream loop in our simulations) being advected over and within the other loop, and at the same time being weakened due to scrunching. The pairing then resembles leap-frogging vortex rings.

The second difference in three-dimensions is that other processes often occur on faster timescales within the loops and disrupt them before the pairing can proceed very far. For example, on some occasions we observe twist waves (both $m = 0$ and $m = 2$) fragmenting and unravelling the vortices while they are pairing. Pairing is less disrupted if it takes place at small scales; presumably, twist waves are heavily influenced by viscosity at these scales (as is the pairing) and are unable to compete with the pairing. Furthermore, in a previous simulation employing lower resolution and 25% greater dissipation, the twist waves at this stage of the simulation were somewhat suppressed and the vortex pairing proceeded with less competition. Finally,
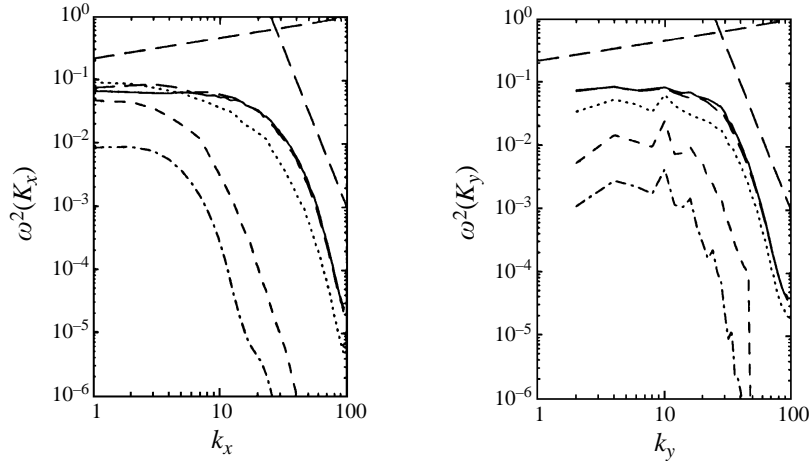
FIGURE 9. Streamwise (*a*) and spanwise (*b*) wavenumber spectra at times of $t = 60$ (dash-dotted), 65 (short dashed), 70 (dotted), 75 (long dashed), and 80 (solid) showing the approach toward isotropy at intermediate and smaller scales of motion. Also shown in each panel are lines having slopes of $+1/3$ and -5.

it is possible that the pairing events facilitate other vortex interactions (e.g. twist waves) by driving the more intense vortex structures closer together.

5. Enstrophy spectra and cascade

The contributions to the k_x and k_y enstrophy spectra from each component of vorticity at $t = 60$, 70, and 80 were presented and discussed in Part 1 and were shown to achieve a significant degree of isotropy at later times. Here we consider only the evolution of the total k_x and k_y enstrophy spectra throughout the simulation. These spectra are shown together at $t = 60$, 65, 70, 75, and 80 in figure 9 to permit a comparison of spectral amplitudes from one time to another. At early times, the flow is clearly anisotropic, as discussed in Part 1. The peaks in the spanwise spectra correspond to the dominant spanwise instability, i.e. the streamwise convective rolls. At later times, the spectra at intermediate and higher wavenumbers tend asymptotically to a single curve. Also, there is close agreement between the streamwise and spanwise spectral shapes and amplitudes at later times. (The absence of enstrophy at k_y greater than 48 at $t = 65$ is because this is the time at which the model fields were interpolated to a finer resolution.) We also show lines having spectral slopes of $+1/3$ and -5 in each panel of figure 9, corresponding to the slopes one might expect for enstrophy in the inertial and viscous ranges of turbulence given energy spectra slopes of $-5/3$ and -7, the -7 being from the Heisenberg model (Heisenberg 1948). In the viscous range, the agreement with the -5 slope is reasonably good, except very near the Nyquist scales where the slope is steeper. In the inertial range, the spectra are flat instead of positively sloped; an exception is at lower wavenumbers and early times in the spanwise spectra where the spectra are positively sloped. The limited extent and slope of the apparent inertial range are likely consequences of a turbulent Reynolds number of 10 or less based on either integral scale or turbulence arguments (Fritts *et al.* 1996). Nevertheless, the clear change in slope in the spectra at $k \sim 30$ is suggestive of the transition from an inertial range to a dissipative range.

6. Summary and conclusions

We have examined the primary and secondary vortex interactions and perturbations accounting for the transition to and the enstrophy cascade within a turbulent flow arising due to the breaking of an internal gravity wave in a stratified and sheared fluid. Our emphasis has been on the vortex dynamics occurring subsequent to the initial wavefield instabilities discussed in Part 1. Vortex interactions judged to be of primary importance in this context include the stretching of vortex structures (sheets and tubes) by nearly orthogonal neighbouring vortex structures, the roll-up of vortex sheets into tubes, and mode-zero and -two twist waves which are excited on the vortex tubes. Other interactions also identified in our simulation, but judged to be of lesser importance in the evolution of the vorticity field, include reconnection, mode-one twist waves, and vortex pairing.

A typical sequence of events begins with orthogonal vortex structures stretching each other. If one of the structures is a vortex sheet, the intensification due to the stretching eventually causes it to roll up into one or more vortex tubes. However, the vortex sheet is finite in extent, and so the resulting vortex tubes have variations in their structure along their axes. These axial variations excite twist waves along the tubes, particularly $m = 0$ and $m = 2$ waves, and these twist waves have such large amplitudes that they fragment, unravel, or burst the tubes on which they propagate. Twist waves can also be excited by interactions of vortex tubes with their neighbours, leading to the same disastrous consequences for the tubes. In this way, the flow evolves from sheets to tubes to tube fragments, each on smaller scales. The process is somewhat self-sustaining as we find that the tube fragments themselves stretch sheets which in turn roll up into new tubes; such processes occur until late in the evolution when the flow is primarily viscously diffusing. Also, mutual stretching events termed x-patterns were found to be relatively stable structures and to persist for long times.

Secondary vortex interactions are evident throughout the flow evolution, but appear to play a less significant role in the cascade of enstrophy toward smaller scales of motion. Reconnection events occur at many sites, although on some occasions apparent reconnection events proved to be nothing more than the intensification of separate portions of a vortex tube which already shared common vorticity fieldlines. Mode-one twist waves are occasionally excited, usually by the effect of an orthogonal neighbouring vortex. These waves were found to be relatively stable and steady, probably because of the steady forcing from the neighbouring tube. Finally, vortex pairing events were observed at several sites in our numerical results and were found to contribute to vortex perturbations leading to their fragmentation and bursting. But the pairing events themselves appeared to play a lesser role than other processes in a less viscous environment.

Perhaps the most significant result of this study is the identification of vortex processes which we believe to be responsible for dynamics within a broad class of turbulent flows. Turbulence has, of course, been studied in many contexts (e.g. in convection, in boundary layers, in strongly rotating fluids, or in our case in a breaking gravity wave), and the details of the transition to turbulence vary according to which flow instabilities contribute to the transition. However, a common feature shared by many, if not all, turbulent flows is the formation of either vortex tubes or vortex loops (i.e. horseshoe or hairpin vortices) (Rogers & Moin 1987; Robinson 1991; Gerz *et al.* 1994; Sandham & Kleiser 1992; Metais *et al.* 1995). Similar structures also occur in the general three-dimensional KH instability (Palmer, Fritts & Andreasson 1996) and in many other flows of sufficiently high Reynolds numbers. The dynamics of the

vortex loops that arise in our current simulation, then, are probably representative of similar dynamics of vortex loops in other flows. For example, the twist waves we observe on vortex loops are caused by axial variations of the vortex loops (see Arendt *et al.* 1997 for a full discussion of this) and by interactions with neighbours. As such variations inevitably occur on finite-length vortex tubes or loops, Kelvin vortex waves and the consequent fragmentation and/or unravelling of the vortex loops should be common in turbulent flows. In fact, double helix unravelling of vortex tubes has been observed by Cadot *et al.* (1995) in laboratory studies of turbulent shear flow. In our flows, we find that twist waves are ubiquitous, and the fragmentation and unravelling of vortex loops that they cause is the predominant fate of the loops; very few vortex loops die a peaceful death by viscous diffusion.

REFERENCES

ANDREASSEN, Ø., HVIDTEN, P. Ø., FRITTS, D. C. & ARENDT, S. 1998 Vorticity dynamics in a breaking gravity wave. Part 1. Initial instability evolution. *J. Fluid Mech.* **367**, 27–46.

ANDREASSEN, Ø., WASBERG, C. E., FRITTS, D. C. & ISLER, J. R. 1994 Gravity wave breaking in two and three dimensions, 1. Model description and comparison of two-dimensional evolutions. *J. Geophys. Res.* **99**, 8095–8108.

ARENDT, S., FRITTS, D. C. & ANDREASSEN, Ø. 1997 The initial value problem for Kelvin vortex waves. *J. Fluid Mech.* **344**, 181–212.

BETCHOV, R. 1957 On the fine structure of turbulent flows. *J. Fluid Mech.* **3**, 205–216.

BORATAV, O. N., PELZ, R. B. & ZABUSKY, N. J. 1992 Reconnection in orthogonally interacting vortex tubes: Direct numerical simulations and quantifications. *Phys. Fluids* A **4**, 581–605.

CADOT, O., DOUADY, S. & COUDER, Y. 1995 Characterization of the low-pressure filaments in a three-dimensional turbulent shear flow. *Phys. Fluids* A **7**, 630–646.

DAVIS, P. A. & PELTIER, W. R. 1979 Some characteristics of the Kelvin-Helmholtz and resonant overreflection modes of shear instability and of their interaction through vortex pairing. *J. Atmos. Sci.* **36**, 2394–2412.

DRAZIN, P. G. 1958 The stability of a shear layer in an unbounded heterogeneous inviscid fluid. *J. Fluid Mech.* **4**, 214–224.

FRITTS, D. C. 1984 Shear excitation of atmospheric gravity waves. Part II: Nonlinear radiation from a free shear layer. *J. Atmos. Sci.* **41**, 524–537.

FRITTS, D. C., GARTEN, J. F. & ANDREASSEN, Ø. 1996 Wave breaking and transition to turbulence in stratified shear flows. *J. Atmos. Sci.* **53**, 1057–1085.

FRITTS, D. C., ISLER, J. R. & ANDREASSEN, Ø. 1994 Gravity wave breaking in two and three dimensions, 2. Three dimensional evolution and instability structure. *J. Geophys. Res.* **99**, 8109–8123.

GERZ, T., HOWELL, J. & MAHRT, L. 1994 Vortex structures and microfronts. *Phys. Fluids* A **6**, 1242–1251.

HEISENBERG, W. 1948 Zur statistischen theorie der turbulenz. *Z. Phys.* **124**, 628–657.

HOPFINGER, E. J., BROWAND, F. K. & GAGNE, Y. 1982 Turbulence and waves in a rotating tank. *J. Fluid Mech.* **125**, 505–534.

ISLER, J. R., FRITTS, D. C. & ANDREASSEN, Ø. 1994 Gravity wave breaking in two and three dimensions, 3. Vortex breakdown and transition to isotropy. *J. Geophys. Res.* **99**, 8125–8137.

JEONG, J. & HUSSAIN, F. 1995 On the identification of a vortex. *J. Fluid Mech.* **285**, 69–94.

KELVIN, LORD 1880 Vibrations of a columnar vortex. *Phil. Mag.* **10**, 155–168.

KIDA, S. & TAKAOKA, M. 1994 Vortex reconnection. *Ann. Rev. Fluid Mech.* **26**, 169–189.

Koop, C. G. & Browand, F. K. 1979 Instability and turbulence in stratified fluid with shear. *J. Fluid Mech.* **93**, 135–159.

Lundgren, T. S. 1982 Strained spiral vortex model for turbulent fine structure. *Phys. Fluids* **25**, 2193–2203.

Maxworthy, T., Hopfinger, E. J. & Redekopp, L. G. 1985 Wave motions on vortex cores. *J. Fluid Mech.* **151**, 141–165.

Melander, M. V. & Hussain, F. 1994 Core dynamics on a vortex column. *Fluid Dyn. Res.* **13**, 1–37.

Melander, M. V. & Hussain, F. 1995 Polarized vorticity dynamics on a vortex column. *Phys. Fluids* A **5**, 1992–2003.

Metais, O., Flores, C., Yanase, S., Riley, J. & Lesieur, M. 1995 Rotating free-shear flows. Part 2. Numerical simulations. *J. Fluid Mech.* **293**, 47–80.

Metcalfe, R. W., Orszag, S. A., Brachet, M. E., Menon, S. & Riley, J. J. 1987 Secondary instability of a temporally growing mixing layer. *J. Fluid Mech.* **184**, 207–243.

Palmer, T. L., Fritts, D. C. & Andreassen, Ø. 1996 Secondary convective and dynamical instabilities of Kelvin-Helmholtz billows in three-dimensional stratified compressible flow. *J. Fluid Mech.* submitted.

Patnaik, P. C., Sherman, F. S. & Corcos, G. M. 1976 A numerical simulation of Kelvin-Helmholtz waves of finite amplitude. *J. Fluid Mech.* **73**, 215–240.

Pumir, A. & Siggia, E. 1990 Collapsing solutions to the 3-D Euler equations. *Phys. Fluids* A **2**, 220–241.

Robinson, S. K. 1991 Coherent motions in the turbulent boundary layer. *Ann. Rev. Fluid Mech.* **23**, 601–639.

Rogers, M. M. & Moin, P. 1987 The structure of the vorticity field in homogeneous turbulent flows. *J. Fluid Mech.* **176**, 33–66.

Saffman, P. G. 1992 *Vortex Dynamics.* Cambridge University Press.

Sandham, N. D. & Kleiser, L. 1992 The late stages of transition to turbulence in channel flow. *J. Fluid Mech.* **245**, 319–348.

Schoppa, W., Hussain, F. & Metcalfe, R. W. 1995 A new mechanism of small scale transition in a plane mixing layer: core dynamics of spanwise vortices. *J. Fluid Mech.* **298**, 23–80.

Scotti, R. S. & Corcos, G. M. 1972 An experiment on the stability of small disturbances in a stratified free shear layer. *J. Fluid Mech.* **52**, 499–528.

She, Z. S., Jackson, E. & Orszag, S. A. 1990 Intermittent vortex structures in homogeneous isotropic turbulence. *Nature* **344**, 226–228.

Shelley, M. J., Meiron, D. I. & Orszag, S. A. 1993 Dynamical aspects of vortex reconnection of perturbed anti-parallel vortex tubes. *J. Fluid Mech.* **246**, 613–652.

Thorpe, S. A. 1985 Laboratory observations of secondary structures in Kelvin–Helmholtz billows and consequences for ocean mixing. *Geophys. Astrophys. Fluid Dyn.* **34**, 175–199.

Vincent, A. & Meneguzzi, M. 1991 The spatial structure and statistical properties of homogeneous turbulence. *J. Fluid Mech.* **225**, 1–20.

Vincent, A. & Meneguzzi, M. 1994 The dynamics of vorticity tubes in homogeneous turbulence. *J. Fluid Mech.* **258**, 245–254.

Winters, K. B. & D'Asaro, E. A. 1994 3D wave breaking near a critical level. *J. Fluid Mech.* **272**, 255–284.